



Fast and Accurate Computation of 3D Charlier Moment Invariants for 3D Image Classification

M. Yamni¹ · A. Daoui² · O. El ogri¹ · H. Karmouni¹ · M. Sayyouri² · H. Qjidaa¹ · M. Maaroufi^{3,4} · B. Alami^{3,4,5}

Received: 19 August 2020 / Revised: 22 May 2021 / Accepted: 30 May 2021 /
Published online: 11 June 2021

© The Author(s), under exclusive licence to Springer Science+Business Media, LLC, part of Springer Nature 2021

Abstract

The problem of 3D digital object invariability is encountered in image processing, especially in pattern classification/recognition. The 3D object should be correctly recognized regardless of its particular position and orientation in the scene. This paper proposes a new method to extract 3D Charlier moment invariants to translation and scaling (3DCMITS). These descriptors are extracted directly from discrete orthogonal Charlier polynomials without using 3D geometric moment invariants. This method is fast and does not require any numerical approximation compared to the indirect method based on 3D geometric moment invariants. The results show the proposed method's effectiveness in terms of speed with an improvement exceeding 99,97%. For validation purposes and as an illustration of the interest of 3DCMITS, this paper offers a classification system for 3D objects based on the proposed 3DCMITS and Support Vector Machine (SVM) classifier. The obtained results are verified with K-Nearest Neighbor (KNN) classifier and other existing works in the literature.

Keywords 3D Charlier moment invariants · 3D Charlier moments · Charlier polynomials · Translation-scale invariance · 3D object classification

Abbreviations

CPs	Charlier Polynomials
3DCMs	3D Charlier Moments
3DCMIT	3D Charlier Moment Invariants to Translation
3DCMIS	3D Charlier Moment Invariants to Scaling
3DCMITS	3D Charlier Moment Invariants to Translation and Scaling
MSE	Mean Square Error

✉ M. Yamni
mohamed.yamni@usmba.ac.ma

Extended author information available on the last page of the article

3DMRI	3D Magnetic Resonance Image
ETIR	Execution Time Improvement Ratio
SVM	Support Vector Machine
KNN	K-Nearest Neighbor
CRP	Correct Recognition Percentage

1 Introduction

Moments have been used successfully in image processing and pattern classification applications for many years, as discriminative descriptors, not only because of their simplicity but also for the extraordinary variety of subjects and applications where they are enlightened. Moments are used to characterize different types of 2D and 3D images in many applications such image analysis [19, 24, 32, 41], pattern recognition [1, 8, 11, 17, 27], face recognition [9], image reconstruction [6, 28, 35], image watermarking [36, 38, 39], image compression [22], edge detection [2], medical image analysis [5, 30, 31], stereo image analysis [29, 37, 40].

Among all types of moments, discrete orthogonal moments have considerable properties: they are characterized by low information redundancy and high discriminating power. In addition, they eliminate the need for numerical approximation and precisely satisfy the orthogonal property [41]. Discrete orthogonal moments are defined by projecting an object/image onto a set of discrete orthogonal polynomials. According to the used type of polynomials, various discrete orthogonal moments can be obtained, such as Tchebichef [19], Krawtchouk [41], Charlier [16], Meixner [25], Hahn [43], and Racah moments [44]. In the classification/recognition field of 3D objects, the 3D object must be identified regardless of its position (translated or rotated) and its size (large or small) [10]. Therefore, invariance to geometric transformations is an essential criterion in these areas. This fundamental requirement pushes researchers to extract the invariants of 3D moments. Several works have been proposed in this context. The first work on 3D invariants was published by Sadjadi and Hall [23]. Their results were later rediscovered (with some modifications) by Guo [12]. These authors extracted only the translation, rotation, and scaling invariants from the second order's geometric moments without any possibility of further extension. Many algorithms were later proposed to generalize the computation of 3D geometric invariant moments [26, 33, 34].

At the beginning of the century, several works have been proposed for computing 3D discrete invariant moments. These invariants are algebraically derived from the invariants of 3D geometric moments. This conventional method (also known as the indirect method) has been extended from the 2D case to cover the 3D case. However, the numerical approximations used when calculating the invariants of 3D geometric moments may cause numerical errors in the computed moments. To solve this problem, Hosny [13] calculated the exact values of 2D geometric moments using mathematical integration of the monomial terms over digital image pixels. He also offered the possibility to extend this method to cover the 3D case. This method can be used to reduce numerical approximation errors in the calculation of 3D geometric moment invariants. Even if the numerical approximation errors can be reduced by this method, it is

limited by the high cost of calculation. This makes invariants of 3D moments derived by this method undesirable, especially in real-time systems for which compliance with time constraints is a fundamental criterion. As a solution, the authors in [3, 46], and [42] developed a method to construct the translation and scaling invariants of 2D Legendre, Tchebichef, and Krawtchouk moments, respectively, directly from their corresponding orthogonal polynomials. Later, the authors in [7, 14], and [1] extended this method to derive the translation and scaling invariants of 3D Legendre, Tchebichef, and Krawtchouk moments, respectively.

Among 3D discrete orthogonal moments, the 3D Charlier moments (3DCMs) are defined as the projection of the 3D image/object onto the Charlier polynomials (CPs). The CPs satisfy exactly the orthogonality property in the discrete domain, so the implementation of these polynomials does not require any numerical approximation. In addition, these polynomials are discrete, and 3D digital images/objects also, so there is no discretization error [18]. CPs are defined by the hypergeometric function ${}_2F_0(\cdot)$ unlike the Tchebichef, Krawtchouk, and Hahn polynomials, which are defined by the hypergeometric functions ${}_3F_2(\cdot)$, ${}_2F_1(\cdot)$ and ${}_3F_2(\cdot)$, respectively, which means that CPs are much simpler and contain fewer terms (Pochhammer symbols and factorials) than other types of discrete orthogonal polynomials.

Motivated by the interesting properties of CPs, this paper proposes a fast method for computing 3D Charlier moment invariants to translation and scaling (3DCMITS) directly from CPs. We first develop the translated and scaled CPs by writing them in the form of simple summations. Then, we develop the algebraic expressions existing between the transformed CPs and the normal CPs. Finally, we use these expressions to derive 3DCMITS. This method takes into account the requirements of accuracy and calculation time. It considerably reduces the computation time and does not require any numerical approximation. The experimental results have shown that the proposed calculation method reduces the calculation time with a rate of more than 99,67% compared to the conventional method.

The proposed descriptors can be applied in applications that require invariance to translation and scaling transformations such as 3D object classification, 3D image recognition, and protection of intellectual property of 3D meshes. For validation purposes and as an illustration of the interest of the proposed descriptors, this paper proposes a classification system for 3D objects based on the proposed 3DCMITS and Support Vector Machine (SVM) classifier. The results are verified with K-Nearest Neighbor (KNN) classifier and other existing works in the literature.

The rest of the paper is organized as follows. In Sect. 2, definitions of CPs, 3DCMs and conventional invariants of 3DCMs are presented. Section 3 presents the proposed method for calculating 3DCMITS. Algorithms for calculating translation and scale invariants using the proposed method are also given in this section. Experimental results for evaluating the performance of the proposed descriptors are given in Sect. 5. Section 6 concludes this paper.

2 3D Charlier Moments

In this section, we will present the mathematical framework of the theory of 3D Charlier moments, including the Charlier polynomials, the 3D Charlier moments and the conventional translation and scaling invariants of the 3D Charlier moments.

2.1 Charlier Polynomials

The n th Charlier polynomials (CPs) are defined by using the hypergeometric function as follows [21]:

$$\begin{aligned} C_n^{a_1}(x) &= {}_2F_0(-n, -x; -a_1^{-1}) \\ &= \sum_{k=0}^n \frac{(-n)_k (-x)_k (-a_1^{-1})^k}{k!} \end{aligned} \quad \left| \quad x, n = 0, 1, 2, \dots, \infty \right. \quad (1)$$

where a_1 is restricted to $a_1 > 0$, and ${}_2F_0(\cdot)$ is the hypergeometric function, defined as:

$${}_2F_0(a, b; c) = \sum_{k=0}^n \frac{(a)_k (b)_k (c)^k}{k!} \quad (2)$$

and $(a)_k$ is the Pochhammer symbol, defined as:

$$\begin{aligned} (a)_0 &= 1 \\ (a)_k &= \frac{(a+k-1)!}{(a-1)!}; k \geq 1 \end{aligned} \quad (3)$$

Equation (1) can be rewritten as follows:

$$\begin{aligned} C_n^{a_1}(x) &= \sum_{k=0}^n \frac{n!}{k!(n-k)!(-a_1)^k} \langle x \rangle_k \\ &= \sum_{k=0}^n \alpha_{n,k} \langle x \rangle_k \end{aligned} \quad (4)$$

where $\alpha_{n,k}$ are the coefficients of the CPs given by:

$$\alpha_{n,k} = \frac{n!}{k!(n-k)!(-a_1)^k} \quad (5)$$

and $\langle x \rangle_k$ is the falling factorial defined as [4]:

$$\langle x \rangle_k = \sum_{i=0}^k s(k, i) x^i \quad (6)$$

where $s(k, i)$ are the Stirling numbers of the first kind.

The CPs satisfy the following orthogonal condition:

$$\sum_{x=0}^{\infty} \omega(x) C_n^{a_1}(x) C_m^{a_1}(x) = \rho(n) \delta_{n,m}; n, m \geq 0 \quad (7)$$

where $\omega(x)$ and $\rho(n)$ are the weight function and the squared norm of CPs, respectively, defined as:

$$\omega(x) = \frac{e^{-a_1} a_1^x}{x!} \quad (8)$$

$$\rho(n) = \frac{n!}{a_1^n} \quad (9)$$

The normalized CPs with respect to the norm $\tilde{C}_n^{a_1}(x)$ are defined as:

$$\tilde{C}_n^{a_1}(x) = \frac{C_n^{a_1}(x)}{\sqrt{\rho(n)}} \quad (10)$$

To obtain numerical stability, the weighted CPs $\bar{C}_n^{a_1}(x)$ are used. They are defined as follows:

$$\bar{C}_n^{a_1}(x) = C_n^{a_1}(x) \sqrt{\frac{\omega(x)}{\rho(n)}} \quad (11)$$

The CPs satisfy the following recurrence relationship [45]:

$$\bar{C}_n^{a_1}(x) = -\sqrt{\frac{a_1}{n}} \frac{(x-n+1-a_1)}{a_1} \bar{C}_{n-1}^{a_1}(x) - \sqrt{\frac{a_1^2}{n(n-1)}} \frac{(n-1)}{a_1} \bar{C}_{n-2}^{a_1}(x) \quad (12)$$

where

$$\bar{C}_0^{a_1}(x) = \sqrt{\frac{\omega(x)}{\rho(0)}} \text{ and } \bar{C}_1^{a_1}(x) = \frac{a_1-x}{a_1} \sqrt{\frac{\omega(x)}{\rho(1)}} \quad (13)$$

2.2 3D Charlier Moments

Given a 3D image/object $I(x, y, z)$ with size $N \times M \times K$, the $(n+m+k)$ order 3D Charlier moments (3DCMs) of the image/object $I(x, y, z)$ are defined as follows:

$$CM_{n,m,k} = \sum_{x=0}^{N-1} \sum_{y=0}^{M-1} \sum_{z=0}^{K-1} \bar{C}_n^{a_1}(x) \bar{C}_m^{a_1}(y) \bar{C}_k^{a_1}(z) I(x, y, z) \quad (14)$$

Equation (7) leads to the following inverse transform

$$I_{rec}(x, y, z) = \sum_{n=0}^{N-1} \sum_{m=0}^{M-1} \sum_{k=0}^{K-1} \bar{C}_n^{a_1}(x) \bar{C}_m^{a_1}(y) \bar{C}_k^{a_1}(z) CM_{n,m,k} \quad (15)$$

where $I_{rec}(x, y, z)$ is the reconstructed 3D image/object.

The difference between the original image/object $I(x, y, z)$ and the reconstructed one $I_{rec}(x, y, z)$ is measured by the Mean Square Error (MSE), which is defined as follows:

$$MSE = \frac{1}{N \times M \times K} \sum_{x=0}^{N-1} \sum_{y=0}^{M-1} \sum_{z=0}^{K-1} (I(x, y, z) - I_{rec}(x, y, z))^2 \quad (16)$$

The 3DCMs presented in this subsection are not invariant under the geometric transformations, such as translation and uniform/non-uniform scaling. In the next subsection, we present the conventional method for deriving the translation and scaling invariants of 3D Charlier moments.

2.3 Derivation of Translation and Scaling Invariants of 3D Charlier Moments Using 3D Geometric Moments

The conventional method to obtain the translation and scaling invariants of 3D Charlier moments is to derive them algebraically from the corresponding invariants of 3D geometric moments. This conventional method is called the indirect method. This subsection provides a brief introduction of this method.

The 3DCMs of a normalized image/object $\hat{I}(x, y, z) = [\omega(x)\omega(y)\omega(z)]^{-1/2}I(x, y, z)$ can be developed as follows:

$$\begin{aligned} CM_{n,m,k} &= \sum_{x=0}^{N-1} \sum_{y=0}^{M-1} \sum_{z=0}^{K-1} \bar{C}_n^{a_1}(x) \bar{C}_m^{a_1}(y) \bar{C}_k^{a_1}(z) \hat{I}(x, y, z) \\ &= \sum_{x=0}^{N-1} \sum_{y=0}^{M-1} \sum_{z=0}^{K-1} \tilde{C}_n^{a_1}(x) \tilde{C}_m^{a_1}(y) \tilde{C}_k^{a_1}(z) I(x, y, z) \\ &= [\rho(n)\rho(m)\rho(k)]^{-1/2} \sum_{x=0}^{N-1} \sum_{y=0}^{M-1} \sum_{z=0}^{K-1} C_n^{a_1}(x) C_m^{a_1}(y) C_k^{a_1}(z) I(x, y, z) \\ &= [\rho(n)\rho(m)\rho(k)]^{-1/2} \sum_{q=0}^n \sum_{l=0}^m \sum_{r=0}^k \chi_{n,q} \chi_{m,l} \chi_{k,r} m_{q,l,r} \end{aligned} \quad (17)$$

where $\chi_{n,i}$ are coefficients of CPs, defined as

$$\chi_{n,i} = \sum_{k=0}^{n-i} \alpha_{n,n-k} s(n-k, i) \quad (18)$$

and $m_{q,l,r}$ are the 3D geometric moments (3DGMs) of order $(q + l + r)$ of the 3D image/object $I(x, y, z)$. The 3DGMs are defined using the discrete approximation as follows [10]:

$$m_{q,l,r} = \sum_{x=0}^{N-1} \sum_{y=0}^{M-1} \sum_{z=0}^{K-1} x^q y^l z^r I(x, y, z) \tag{19}$$

The 3D geometric moment invariants to translation (3DGMIT) $\mu_{n,m,k}$ (also called the central geometric moments) are defined as follows [10]:

$$\begin{aligned} \mu_{n,m,k} &= \sum_{x=0}^{N-1} \sum_{y=0}^{M-1} \sum_{z=0}^{K-1} (x - \bar{x})^n (y - \bar{y})^m (z - \bar{z})^k I(x, y, z) \\ &= \sum_{q=0}^n \sum_{l=0}^m \sum_{r=0}^k \binom{n}{q} \binom{m}{l} \binom{k}{r} (-1)^{q+l+r} (\bar{x})^q (\bar{y})^l (\bar{z})^r m_{n-q,m-l,k-r} \end{aligned} \tag{20}$$

where \bar{x} , \bar{y} , and \bar{z} are the centroid coordinates of the 3D image/object $I(x, y, z)$, defined as:

$$\bar{x} = \frac{m_{1,0,0}}{m_{0,0,0}}, \bar{y} = \frac{m_{0,1,0}}{m_{0,0,0}}, \bar{z} = \frac{m_{0,0,1}}{m_{0,0,0}} \tag{21}$$

The 3DGMIT change in case of uniform/non-uniform scaling of the 3D image/object is expressed as follows:

$$\begin{aligned} \mu'_{n,m,k} &= \sum_{x=0}^{N-1} \sum_{y=0}^{M-1} \sum_{z=0}^{K-1} a^n (x - \bar{x})^n b^m (y - \bar{y})^m c^k (z - \bar{z})^k abc I(x, y, z) \\ &= a^{n+1} b^{m+1} c^{k+1} \mu_{n,m,k} \end{aligned} \tag{22}$$

where a , b , and c are the scaling factors in the x -, y -, and z -direction of the 3D image/object, respectively.

The 3DGM invariants to translation and scaling (3DGMITS), denoted $V_{n,m,k}$, can be obtained using the following normalization [10]:

$$V_{n,m,k} = \frac{\mu_{0,0,0}^{\xi+2}}{\mu_{(n+\xi),0,0} \mu_{0,(m+\xi),0} \mu_{0,0,(k+\xi)}} \cdot \mu_{n,m,k}; \xi = 0, 1, 2, \dots \tag{23}$$

If we replace the 3DGMs $m_{q,l,r}$ in Eq. (17) by 3DGMIT $\mu_{q,l,r}$ and by 3DGMITS $V_{q,l,r}$, we obtain the 3D Charlier moment invariants to translation (3DCMIT) and 3D Charlier moment invariants to translation and scaling (3DCMITS), respectively. However, this indirect method has two major drawbacks:

- It is dependent on the numerical approximations used during the calculation of 3DGMIT in Eq. (20) and 3DGMITS in Eq. (23) which produces approximation errors.
- It needs a lot of time to extract the 3DCMITS, because the coefficients of the CPs $\alpha_{n,k}$ are time consuming.

These drawbacks limit the use of the indirect method: The first drawback can influence the accuracy of the results in all applications where 3DCMITS can be applied such as object classification, image recognition, and digital watermarking of 3D meshes. The second drawback makes the use of 3DCMITS impossible in real-time systems where compliance with time constraints in the execution of processing is very important, as is the accuracy of these processing results. This paper proposes a quick method to solve these drawbacks, without numerical approximation, to obtain 3DCMITS. This method is presented in the following section.

3 Proposed 3D Charlier Moment Invariants to Translation and Scaling

In this section, we develop a new method to derive the 3D Charlier moment invariants to translation and scaling (3DCMITS). This method uses the particular properties of the Charlier polynomials (CPs) to directly derive the 3DCMITS without going through the computation of 3D geometric moments (3DGMs). In the first subsection, we present the mathematical framework for algebraically deriving the 3D Charlier moment invariants to translation (3DCMIT), while in the second subsection, we derive the 3D Charlier moment invariants to scaling (3DCMIS). Finally, we offer in the third subsection the algorithms for calculating these descriptors.

3.1 3D Charlier Moment Invariants to Translation

The 3DCMIT of order $(n + m + k)$ are noted ‘‘ $\varphi_{n,m,k}$ ’’ for abbreviation.

For a normalized 3D image/object $\hat{I}(x, y, z) = [\omega(x)\omega(y)\omega(z)]^{-1/2}I(x, y, z)$, the direct definition of 3DCMIT can be achieved simply by shifting the origin of coordinates at the image/object centroid, as following:

$$\varphi_{n,m,k} = \sum_{x=0}^{N-1} \sum_{y=0}^{M-1} \sum_{z=0}^{K-1} \tilde{C}_n^{a_1}(x - \bar{x}) \tilde{C}_m^{a_1}(y - \bar{y}) \tilde{C}_k^{a_1}(z - \bar{z}) I(x, y, z) \tag{24}$$

where \bar{x} , \bar{y} and \bar{z} are given in Eq. (22).

In the following, we will establish the relations between the translated CPs $\{C_n^{a_1}(x - \bar{x}), C_m^{a_1}(y - \bar{y}), C_k^{a_1}(z - \bar{z})\}$ and the normal CPs $\{C_n^{a_1}(x), C_m^{a_1}(y), C_k^{a_1}(z)\}$. In this development, we are only interested in CPs translated in the x -direction, where the results found can be obtained in the same way for CPs translated in the y - and z -direction, respectively.

Using Eq. (4), the CPs translated in the x -direction can be developed as follows:

$$\begin{aligned} C_n^{a_1}(x - \bar{x}) &= \sum_{k=0}^n \alpha_{n,k} \langle x - \bar{x} \rangle_k \\ &= \alpha_{n,n} \langle x - \bar{x} \rangle_n + \alpha_{n,n-1} \langle x - \bar{x} \rangle_{n-1} + \alpha_{n,n-2} \langle x - \bar{x} \rangle_{n-2} \\ &\quad + \alpha_{n,n-3} \langle x - \bar{x} \rangle_{n-3} \dots + \alpha_{n,k} \langle x - \bar{x} \rangle_k \end{aligned} \tag{25}$$

where

$$\langle x - \bar{x} \rangle_k = \sum_{l=0}^k \binom{k}{l} \langle \bar{x} \rangle_l \langle x \rangle_{k-l} \tag{26}$$

Using Eq. (26), the CPs translated in the x -direction become:

$$\begin{aligned} C_n^{a_1}(x - \bar{x}) &= \alpha_{n,n} \langle x \rangle_n \\ &+ \left[\alpha_{n,n-1} + \alpha_{n,n} \binom{n}{1} \langle -\bar{x} \rangle_1 \right] \langle x \rangle_{n-1} \\ &+ \left[\alpha_{n,n-2} + \alpha_{n,n-1} \binom{n-1}{1} \langle -\bar{x} \rangle_1 + \alpha_{n,n} \binom{n}{2} \langle -\bar{x} \rangle_2 \right] \langle x \rangle_{n-2} \\ &+ \left[\alpha_{n,n-3} + \alpha_{n,n-2} \binom{n-2}{1} \langle -\bar{x} \rangle_1 + \alpha_{n,n-1} \binom{n-1}{2} \langle -\bar{x} \rangle_2 + \alpha_{n,n} \binom{n}{3} \langle -\bar{x} \rangle_3 \right] \langle x \rangle_{n-3} \\ &+ \dots \end{aligned} \tag{27}$$

Substituting the normal CPs into the series of decreasing falling factorials of x , we find the following expression:

$$C_n^{a_1}(x - \bar{x}) = \sum_{k=0}^n v_{n,n-k}(-\bar{x}) C_{n-k}^{a_1}(x) \tag{28}$$

where

$$\begin{aligned} v_{n,n}(-\bar{x}) &= 1 \\ v_{n,n-k}(-\bar{x}) &= \frac{1}{\alpha_{n-k,n-k}} \left[\sum_{l=0}^k \binom{n-k+l}{l} \alpha_{n,n-k+l} \langle -\bar{x} \rangle_l - \sum_{i=0}^{k-1} \alpha_{n-i,n-k} v_{n,n-i}(-\bar{x}) \right]; k \leq n \end{aligned} \tag{29}$$

The following relationships can be taken from Eq. (29):

$$v_{n,n}(-\bar{x}) = 1 \tag{30}$$

$$v_{n,n-1}(-\bar{x}) = \frac{n}{(-a_1)} \langle -\bar{x} \rangle_1 \tag{31}$$

$$v_{n,n-2}(-\bar{x}) = \frac{n(n-1)}{2(a_1)^2} \langle -\bar{x} \rangle_2 \tag{32}$$

$$v_{n,n-3}(-\bar{x}) = \frac{n(n-1)(n-2)}{3!(-a_1)^3} \langle -\bar{x} \rangle_3 \tag{33}$$

$$v_{n,n-4}(-\bar{x}) = \frac{n(n-1)(n-2)(n-3)}{4!(-a_1)^4} \langle -\bar{x} \rangle_4 \tag{34}$$

By examining Eqs. (30–34), we find that the expression $v_{n,n-k}(-\bar{x})$ can be written in the following form:

$$\begin{aligned} v_{n,n-k}(-\bar{x}) &= \frac{n(n-1)(n-2)\dots(n-k+1)}{k!(-a_1)^k} \langle -\bar{x} \rangle_k \\ &= \frac{\langle n \rangle_k}{k!(-a_1)^k} \langle -\bar{x} \rangle_k = f(n, k) \langle -\bar{x} \rangle_k \end{aligned} \tag{35}$$

where

$$f(n, k) = \frac{\langle n \rangle_k}{k!(-a_1)^k} \tag{36}$$

Since we are interested in the normalized CPs defined by Eq. (10), we will generalize Eqs. (35) and (36).

By using Eqs. (4) and (10), the normalized normal CPs $\tilde{C}_n^{a_1}(x)$ and the normalized translated CPs $\tilde{C}_n^{a_1}(x - \bar{x})$ are expressed as follows:

$$\tilde{C}_n^{a_1}(x) = \sum_{k=0}^n \tilde{\alpha}_{n,n-k} \langle x \rangle_k \tag{37}$$

$$\tilde{C}_n^{a_1}(x - \bar{x}) = \sum_{k=0}^n \tilde{v}_{n,n-k}(-\bar{x}) \tilde{C}_{n-k}^{a_1}(x) \tag{38}$$

where

$$\tilde{\alpha}_{n,n-k} = \frac{\alpha_{n,k}}{\sqrt{\rho(n)}} \tag{39}$$

$$\tilde{v}_{n,n-k}(-\bar{x}) = \frac{1}{\tilde{\alpha}_{n-k,n-k}} \left[\sum_{l=0}^k \binom{n-k+l}{l} \tilde{\alpha}_{n,n-k+l} \langle -\bar{x} \rangle_l - \sum_{i=0}^{k-1} \tilde{\alpha}_{n-i,n-k} \tilde{v}_{n,n-i}(-\bar{x}) \right] \tag{40}$$

Using Eqs. (38) and (40), the following expression can be derived using the same procedures as in Eq. (38):

$$\tilde{v}_{n,n-k}(-\bar{x}) = \tilde{f}(n, k) \langle -\bar{x} \rangle_k \tag{41}$$

where

$$\tilde{f}(n, k) = \frac{\langle n \rangle_k}{k!(-a_1)^k} \sqrt{\frac{\rho(n-k)}{\rho(n)}}; k \leq n \tag{42}$$

Finally, the normalized translated CPs can be expressed in terms of normalized normal CPs as follows:

$$\tilde{C}_n^{a_1}(x - \bar{x}) = \sum_{q=0}^n \tilde{f}(n, k) \langle -\bar{x} \rangle_q \tilde{C}_{n-q}^{a_1}(x) \tag{43}$$

The result of Eq. (43) can also be generalized for normalized translated CPs in the y and z directions as follows:

$$\tilde{C}_m^{a_1}(y - \bar{y}) = \sum_{l=0}^m \tilde{f}(m, l) \langle -\bar{y} \rangle_l \tilde{C}_{m-l}^{a_1}(y) \tag{44}$$

$$\tilde{C}_k^{a_1}(z - \bar{z}) = \sum_{r=0}^k \tilde{f}(k, r) \langle -\bar{z} \rangle_r \tilde{C}_{k-r}^{a_1}(z) \tag{45}$$

By substituting Eqs. (43) - (45) in Eq. (24), the 3DCMIT become:

$$\varphi_{n,m,k} = \sum_{q=0}^n \sum_{l=0}^m \sum_{r=0}^k \tilde{f}(n, q) \tilde{f}(m, l) \tilde{f}(k, r) \langle -\bar{x} \rangle_q \langle -\bar{y} \rangle_l \langle -\bar{z} \rangle_r CM_{n-q, m-l, k-r} \tag{46}$$

Eq. (46) shows that 3DCMIT are derived directly from 3DCMs.

It should be noted that the expression $\tilde{f}(\cdot)$ in Eq. (46) is independent of the 3D image/object. Therefore, this expression can be pre-computed, stored, recalled whenever it is needed to avoid repetitive computation.

3.2 3D Charlier Moment Invariants to Scaling

Either a 3D image/object is scaled non-uniformly with the scaling factors a, b and c in the x -, y - and z -direction, respectively, the 3DCMs are changed as follows:

$$CM'_{n,m,k} = abc \sum_{x=0}^{N-1} \sum_{y=0}^{M-1} \sum_{z=0}^{K-1} \tilde{C}_n^{a_1}(ax) \tilde{C}_m^{a_1}(by) \tilde{C}_k^{a_1}(cz) I(x, y, z) \tag{47}$$

In the following, we will establish the relations between the normalized scaled CPs $\{\tilde{C}_n^{a_1}(ax), \tilde{C}_m^{a_1}(by), \tilde{C}_k^{a_1}(cz)\}$ and the normalized normal CPs $\{\tilde{C}_n^{a_1}(x), \tilde{C}_m^{a_1}(y), \tilde{C}_k^{a_1}(z)\}$. We are interested in this development only in the normalized CPs scaled in the x -direction, where the results found can be obtained in the same way for the normalized CPs scaled in the y - and z -direction, respectively.

The normalized CPs scaled in the x -direction can be expressed as a series of decreasing powers of x , using Eqs. (7) and (5), as follows:

$$\begin{aligned}
 \tilde{C}_n^{a_1}(ax) &= \sum_{k=0}^n \tilde{\alpha}_{n,k} \langle ax \rangle_k = \sum_{k=0}^n \tilde{\alpha}_{n,k} \sum_{i=0}^k s(k, i) a^i x^i \\
 &= \sum_{k=0}^n \sum_{i=0}^k \tilde{\alpha}_{n,n-k} s(k, i) a^i x^i = \sum_{i=0}^n \sum_{k=0}^{n-i} \tilde{\alpha}_{n,n-k} s(n-k, i) a^i x^i \\
 &= \sum_{i=0}^n \tilde{\chi}_{n,i} a^i x^i
 \end{aligned} \tag{48}$$

where

$$\chi_{n,i} = \sum_{k=0}^{n-i} \tilde{\alpha}_{n,n-k} s(n-k, i) \tag{49}$$

It can be easily deduced from Eq. (48) the relationship between $\tilde{C}_n^{a_1}(ax)$ and $\tilde{C}_n^{a_1}(x)$ as follows:

$$\sum_{q=0}^n \gamma_{n,q} \tilde{C}_q^{a_1}(ax) = a^n \sum_{q=0}^n \gamma_{n,q} \tilde{C}_q^{a_1}(x) \tag{50}$$

where

$$\begin{aligned}
 \gamma_{n,n} &= 1 \\
 \gamma_{n,q} &= \sum_{i=0}^{n-q-1} -\frac{\chi_{n-i,q} \gamma_{n,n-i}}{\chi_{q,q}}
 \end{aligned} \tag{51}$$

The normalized CPs scaled in the y- and z-direction can also be expressed as a function of normalized normal CPs as follows:

$$\sum_{l=0}^m \gamma_{m,l} \tilde{C}_l^{a_1}(by) = b^m \sum_{l=0}^m \gamma_{m,l} \tilde{C}_l^{a_1}(y) \tag{52}$$

$$\sum_{r=0}^k \gamma_{k,r} \tilde{C}_r^{a_1}(cz) = c^k \sum_{r=0}^k \gamma_{k,r} \tilde{C}_r^{a_1}(z) \tag{53}$$

From Eqs. (47), (50), (52), (53), we deduce the relationship between scaled 3DCMs and normal 3DCMs:

$$\begin{aligned}
 \Psi_{n,m,k} &= \sum_{q=0}^n \sum_{l=0}^m \sum_{r=0}^k \gamma_{n,q} \gamma_{m,l} \gamma_{k,r} CM'_{q,l,r} \\
 &= a^{n+1} b^{m+1} c^{k+1} \sum_{q=0}^n \sum_{l=0}^m \sum_{r=0}^k \gamma_{n,q} \gamma_{m,l} \gamma_{k,r} CM_{q,l,r}
 \end{aligned} \tag{54}$$

The following relationships can be drawn from Eq. (54):

$$\begin{aligned}
 1) \psi_{0,0,0} &= abcCM_{0,0,0} \\
 2) \psi_{n,0,0} &= a^{n+1}bc \sum_{q=0}^n \gamma_{n,q} CM_{q,0,0} \\
 3) \psi_{0,m,0} &= ab^{m+1}c \sum_{l=0}^m \gamma_{m,l} CM_{0,l,0} \\
 4) \psi_{0,0,k} &= abc^{k+1} \sum_{r=0}^k \gamma_{k,r} CM_{0,0,k}
 \end{aligned} \tag{55}$$

The scaling factors (a , b , and c) in $\psi_{n,m,k}$ can be canceled using the following normalization:

$$\phi_{n,m,k} = \frac{\psi_{n,m,k} \psi_{0,0,0}^{\xi+2}}{\psi_{(n+\xi),0,0} \psi_{0,(m+\xi),0} \psi_{0,0,(k+\xi)}}; \xi = 0, 1, 2, \dots \tag{56}$$

The $\phi_{n,m,k}$ are uniform/non-uniform scaling invariants of 3D Charlier moments.

Proof Let $\phi'_{n,m,k}$ denotes the scaled version of $\phi_{n,m,k}$, the relationship between them is:

$$\begin{aligned}
 \phi'_{n,m,k} &= \frac{\psi'_{n,m,k} \psi'^{\xi+2}_{0,0,0}}{\psi'_{(n+\xi),0,0} \psi'_{0,(m+\xi),0} \psi'_{0,0,(k+\xi)}} \\
 &= \frac{a^{n+1} b^{m+1} c^{k+1} \psi_{n,m,k} a^{\xi+2} b^{\xi+2} c^{\xi+2} \psi_{0,0,0}^{\xi+2}}{a^{n+1+\xi} b^{\xi} c^{\xi} \psi_{(n+\xi),0,0} a^{\xi} c^{\xi} b^{m+1+\xi} \psi_{0,(m+\xi),0} a^{\xi} b^{\xi} c^{k+1+\xi} \psi_{0,0,(k+\xi)}} \tag{57} \\
 &= \frac{\psi_{0,0,0}^{\xi+2}}{\psi_{(n+\xi),0,0} \psi_{0,(m+\xi),0} \psi_{0,0,(k+\xi)}} \cdot \psi_{n,m,k} \\
 &= \phi_{n,m,k}
 \end{aligned}$$

The proof is completed.

Eq. (56) shows that 3DCMIS are directly derived from 3DCM.

3.3 Algorithms

After having calculated 3DCMIT and 3DCMIS by the proposed method, we summarize the steps for calculating these descriptors in the algorithms 1 and 2.

Algorithm 1: Computation of 3D Charlier moment invariants to translation (3DCMIT).

For given 3D image/object $I(x, y, z)$ with size $N \times M \times K$	
Step 1	Computation of Charlier polynomials $\bar{C}_n^{a_i}(x)$ using Eqs. (12) and (13).
Step 2	Compute the 3D Charlier moment of the order $(m+n+k)$ using Eq. (14).
Step 3	Compute the centroid coordinates of 3D image/object $I(x, y, z)$ \bar{x} , \bar{y} , and \bar{z} using Eq. (21).
Step 4	Compute the expression $\tilde{f}(\cdot)$ Eq. (42).
Step 5	Finally, calculate $\varphi_{n,m,k}$ using Eq. (46).

Algorithm 2: Computation of 3D Charlier moment invariants to scaling (3DCMIS).

For given 3D image/object $I(x, y, z)$ with size $N \times M \times K$	
Step 1	Compute the Charlier polynomials $\bar{C}_n^{a_i}(x)$ using Eqs. (12) and (13).
Step 2	Compute the 3D Charlier moments of the order $(m+n+k)$ using Eq. (14).
Step 3	Compute the expression $\gamma_{n,q}$ using Eq. (51).
Step 4	Compute the invariants $\psi_{n,m,k}$ using Eq. (54).
Step 5	Finally, calculate $\phi_{n,m,k}$ using Eq. (56).

The algorithms 1 and 2 can be combined to obtain the 3D Charlier moment invariants to translation and scaling (3DCMITS). The 3DCMITS of order $(n+m+k)$ are noted " $\Phi_{n,m,k}$ " for abbreviation.

4 Experimental Results

In this section, we give experimental results to validate the performance of the proposed descriptors. This section is divided into four subsections. In the first subsection, we test the ability of 3DCMs to reconstruct 3D images/objects. In the second subsection, we evaluate and compare the invariability of 3DCMIT and 3DCMIS derived by the proposed method and by the indirect method. In the third subsection, we compare the calculation time of 3DCMIT and 3DCMIS by the proposed method and the indirect method. In the last subsection, we present a classification system for 3D objects based on the proposed 3DCMITS and the SVM and KNN classifiers in both noise-free and noisy conditions.

4.1 3D object reconstruction using 3D Charlier Moments

The reconstruction of the original image/object from a set of its moments has been discussed in the literature quite often, because the reconstruction abilities of moments are connected with their classification power. Studying the image/object

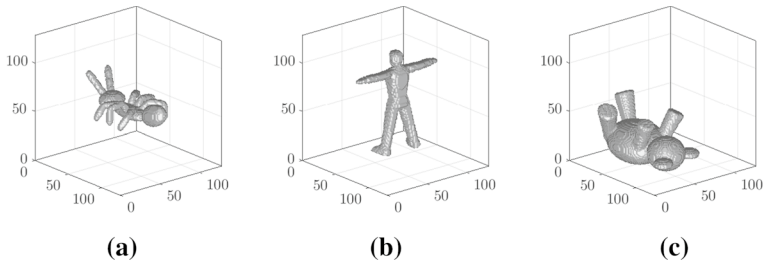
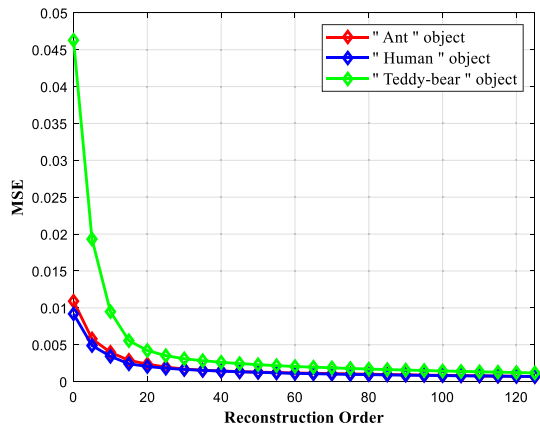


Fig. 1 Original 3D objects of size $128 \times 128 \times 128$; **a** "Ant", **b** "Human", and **c** "Teddy-bear "

Fig. 2 MSE of "Ant", "Human", and "Teddy-bear" 3D objects using 3DCMs



reconstruction problem provides an insight into moment properties that are important for classification without performing classification experiments. That's why so many authors have discussed image reconstruction from different moments in their papers [10]. In this subsection, we show the ability of 3DCMs to reconstruct 3D images/objects. In the first test, we use three objects "Ant", "Human", and "Teddy-bear" of size $128 \times 128 \times 128$ (Fig. 1) extracted from the McGill 3D Shape Benchmark database [47]. The reconstruction tests are performed using 3DCMs with various values of moment order, ranging from 1 up to 125. Figure 2 shows the MSEs between the original objects and the reconstructed ones according to the reconstruction order ranging from 1 to 125. A set of reconstructed objects is shown in Fig. 3. Figure 2 show that MSEs decrease with increasing order of reconstruction. It is also shown that from order 60 ($n = 20$, $m = 20$, $k = 20$) the MSEs tend toward zero, which means that the reconstructed objects are very similar to the original ones. This is clearly shown in Fig. 3. These results show the ability of the 3DCMs to reconstruct 3D objects from a limited number of moments. Therefore, the lower order 3DCMs can replace a 3D object in all applications in order to reduce processing time.

In the second test, we compare the ability of 3DCMs to reconstruct 3D medical images. For this, we use a 3D Magnetic Resonance Image (3DMRI) of size $100 \times 100 \times 100$ which is shown in Fig. 4. The capacity of 3DCMs is compared

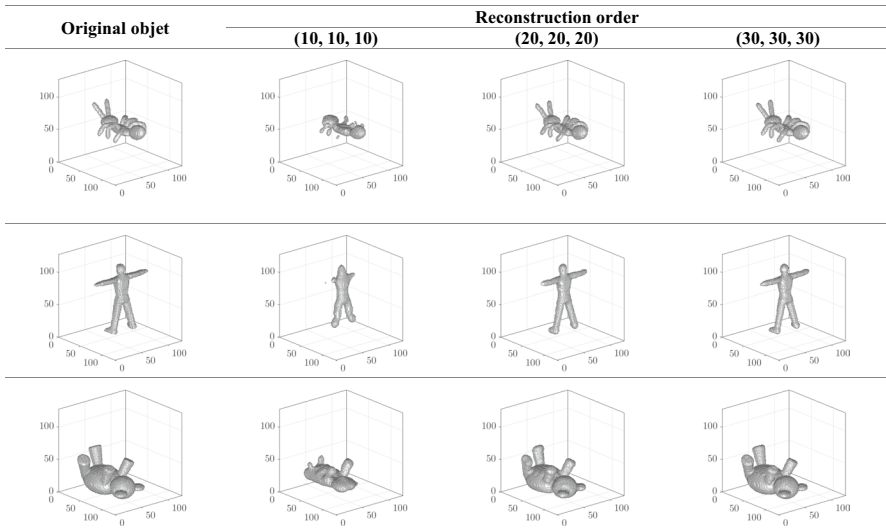
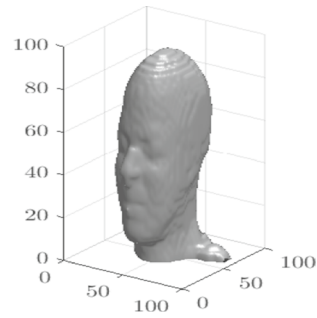


Fig. 3 Reconstruction of "Ant", "Human", and "Teddy-bear " objects using 3DCMs for different classification order

Fig. 4 3D Magnetic Resonance Image (3DMRI) of size $100 \times 100 \times 100$



with that of other types of discrete orthogonal moments, such as 3D Krawtchouk moments (3DKMs), 3D Tchebichef moments (3DTMs), and 3D Hahn moments (3DHMs). Figure 5 shows the results of this comparison. This figure shows that the MSEs of all these moments tend towards zero with the increase in reconstruction order, which means that these moments are able to reconstruct the 3D medical images that have a high degree of complexity. It is also shown that the reconstruction performance of 3DCMs, 3DKMs, 3DTMs, and 3DHMs are very similar to each other, with reconstruction errors of the same order of magnitude (10^{-3}), with a relative advantage of 3DCMs and 3DKMs when using low and high reconstruction orders, respectively. The results of this subsection clearly show that 3DCMs can successfully describe 3D images/objects with a limited number of orders, which means that these descriptors are desirable in applications that suffer from computational complexity.

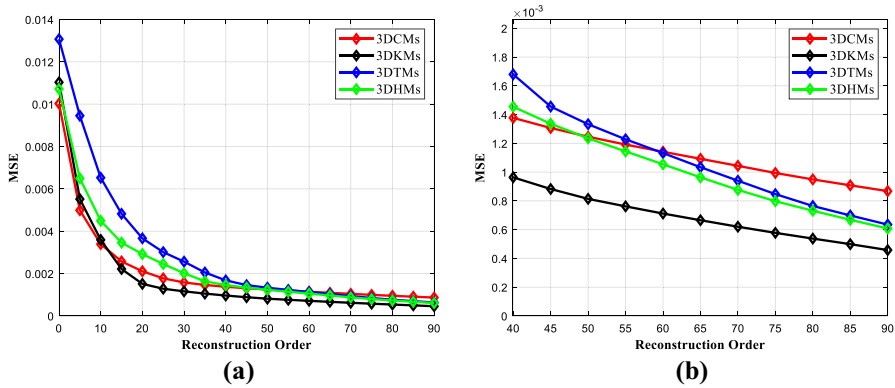


Fig. 5 **a** Comparison of the reconstruction errors for 3DMRI by using 3DCMs, 3DKMs, 3DTMs, and 3DHMs. **b** Enlarge part of (a)

4.2 Invariability

In this subsection, we test the invariability of the proposed 3DCMIT and 3DCMIS under the geometric transformations of translation and uniform/non-uniform scaling. For this purpose, two 3D objects "Four" and "Airplane" (Fig. 6) of size $128 \times 128 \times 128$ extracted from the McGill 3D Shape Benchmark database [47], are used as test objects. In order to measure the capacity of the proposed invariants to remain unchanged under the translation and uniform/non-uniform scaling, we use as objective criterion the deviation of the moments, which is defined as follows:

$$X = \frac{\sigma}{|\mu|} \times (100\%) \tag{58}$$

where σ and μ denotes the standard deviation and the mean of the 3D Charlier moment invariants, respectively. The small value of deviation X indicates that the invariants of the 3D Charlier moments are robust with respect to the translation

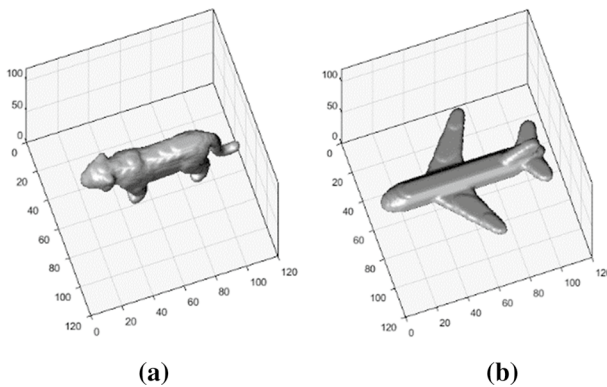


Fig. 6 The 3D test object in subsection 4.2: **a** "Four", **b** "Airplane"

and uniform/non-uniform scaling. The parameter of CPs a_1 is fixed at the value $(N + M + K)/3$, where $N \times M \times K$ is the size of 3D object, and the invariants of 3D Charlier moments are calculated up to order three in this subsection.

In the first test, we check the efficiency of the 3DCMIT descriptors constructed via Eq. (46). The original 3D object "Four" shown in Fig. 6a is translated with a set of translation vectors in the x -, y -, and z -direction. Fig. 7 shows a set of translated objects. The values of the 3DCMIT of some orders are presented in Table 1. It can be seen from this table that the deviation X of the values of the 3DCMIT is equal to zero, which means that the 3DCMIT remain unchanged whatever the translation effected to 3D object. Therefore, 3DCMIT are very robust against 3D object translation.

In the second test, we check the effectiveness of the proposed 3DCMIS descriptors constructed via Eq. (56). The original object "Four" is scaled non-uniformly in the x -, y -, and z -direction. Figure 8 shows a set of scaled "Four" object. Table 2 shows the values of 3DCMIS. This table clearly shows that the values of 3DCMIS remain unchanged under different non-uniform scaling transformations and that the deviation X is equal to zero, which proves the robustness of 3DCMIS with respect to the uniform/non-uniform scaling transformation.

In the last test, we compare the invariability of the 3DCMITS by two methods: the indirect method based on Eq. (23), and the proposed method based on Eqs. (46) and (56). The 3D object "Airplane" presented in Fig. 6b is transformed by a set of mixed translation and scaling transformations. A set of transformed 3D "Airplane" objects is shown in Fig. 9. Table 3 shows the values of 3DCMITS obtained by the two methods. From Table 3 we can see that the deviation X of the proposed 3DCMITS are very small (10^{-10}) under the mixed transformations of translation and scaling, which shows that the 3DCMITS values of the transformed objects are very similar and almost identical to each other. In addition, the proposed 3DCMITS are very robust compared to the 3DCMITS derived from the indirect method which gives a deviation X of order 10^{-4} . Therefore, the proposed method offers better robustness against translation and scaling transformations than the indirect method. These satisfactory results are obtained thanks to the adopted strategy of extracting these invariants which does not require any numerical approximation, thus increasing the computational accuracy of 3DCMITS.

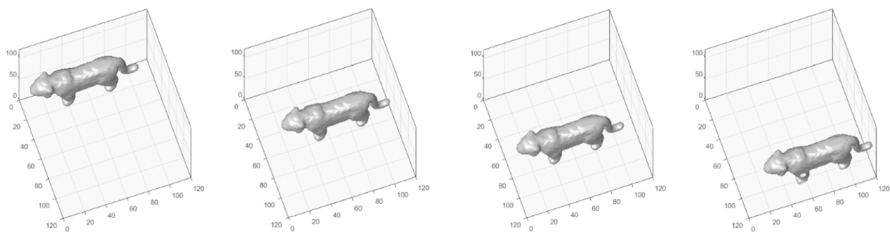


Fig. 7 Set of translated 3D "Four" object

Table 1 Invariability of the proposed 3DCMIT

Translation	$\varphi_{1,2,0}$	$\varphi_{2,1,0}$	$\varphi_{1,2,1}$	$\varphi_{2,1,1}$	$\varphi_{3,0,0}$	$\varphi_{1,3,1}$	$\varphi_{3,1,1}$
$\Delta i = -10; \Delta j = -6; \Delta k = -10$	6,37297E-13	6,46630E-13	-1,57721e-14	1,51089E-4	1,97,999 E-4	1,53,669 E-4	1,84,049 E-4
$\Delta i = +8; \Delta j = +10; \Delta k = +10$	6,37297E-13	6,46630E-13	-1,57721e-14	1,51089E-4	1,97,999 E-4	1,53,669 E-4	1,84,049 E-4
$\Delta i = +10; \Delta j = +8; \Delta k = -10$	6,37297E-13	6,46630E-13	-1,57721e-14	1,51089E-4	1,97,999 E-4	1,53,669 E-4	1,84,049 E-4
$\Delta i = -10; \Delta j = +10; \Delta k = -8$	6,37297E-13	6,46630E-13	-1,57721e-14	1,51089E-4	1,97,999 E-4	1,53,669 E-4	1,84,049 E-4
$\Delta i = -6; \Delta j = +8; \Delta k = +10$	6,37297E-13	6,46630E-13	-1,57721e-14	1,51089E-4	1,97,999 E-4	1,53,669 E-4	1,84,049 E-4
$\Delta i = +6; \Delta j = +10; \Delta k = +6$	6,37297E-13	6,46630E-13	-1,57721e-14	1,51089E-4	1,97,999 E-4	1,53,669 E-4	1,84,049 E-4
$X = \sigma/\mu(\%)$	0	0	0	0	0	0	0

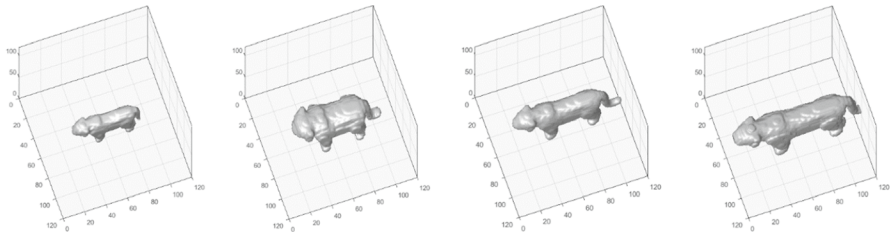


Fig. 8 Set of scaled 3D "Four" object

4.3 The Computational Time of 3DCMITS

In this subsection, we evaluate the computation time of 3DCMIT and 3DCMIS. In the first test, we compare the computation time of 3D Charlier moment invariants using the proposed method and the indirect method. The Execution Time Improvement Ratio (ETIR) [15] is used as a criterion in this comparison. This ratio is defined as $ETIR(\%) = (1 - \text{Time1}/\text{Time2}) \times 100$, where Time1 and Time2 are the execution time of the proposed method and the indirect method, respectively. Both methods are identical in terms of speed if $ETIR = 0\%$. The three objects of "Ant", "Human", and "Teddy-bear" (Fig. 1) are used as test objects. These objects are transformed with translations $\Delta i = \Delta j = \Delta k$ going from -1 to 2 , and scaled in the x , y and z directions with scaling factors $a = b = c$ going from 0.5 to 2 . The calculation process is performed 10 times for moment orders ranging from 1 to 12, from 1 to 24 and from 1 to 36 for each object. Tables 4 and 5 represent the average calculation time and the $ETIR(\%)$ of 3DCMIT and 3DCMIS, respectively. These tables show that the proposed method is faster than the indirect method with an improvement more than 99.67% . It should be noted that the $ETIR$ is 99.67% for the test of translation invariance and 99.97% for the test of scaling invariance, which proves the effectiveness of the proposed method in terms of speed compared to the indirect method.

In the second test, we evaluate the speed of the proposed 3DCMITS for 3D medical images. For that, the 3DMRI in Fig. 4 is used as a test image. This image is translated with the translation vector $(\Delta i = -10, \Delta j = +6, \Delta k = +10)$ and scaled with the scaling factors $(a = 1.1, b = 0.8, c = 1.4)$. The 3DCMITS based on the proposed method are compared with the 3D Tchebichef moment invariants (3DTMI) and the 3D Krawtchouk moment invariants (3DKMI) which are based on the methods presented in papers [7] and [1], respectively. The speed of these methods is also compared with that of indirect methods. The process of calculating these invariants is carried out 10 times for orders ranging from 0 to 12. The average times and the average $ETIR$ are presented in Table 6. The results of Table 6 clearly indicate that the 3DCMITS based on the proposed method are very fast than those based on the indirect method with an improvement of 99.97% . These results also show that the computation time of 3DCMITS is less than the computation time of 3DTMI and 3DKMI based on the methods presented in [7] and [1], respectively. This may be due to the choice of Charlier polynomials as the basic function where they are defined by the hypergeometric function ${}_2F_0(\cdot)$ which contain fewer Pochhammer

Table 2 Invariability of the proposed 3DCMIS

Scaling	$\varphi_{1,2,0}$	$\varphi_{2,1,0}$	$\varphi_{1,2,1}$	$\varphi_{2,1,1}$	$\varphi_{3,0,0}$	$\varphi_{1,3,1}$	$\varphi_{3,1,1}$
$a = 1.5; b = 0.8; c = 0.7$	-4,51305E-13	3,41754E-14	-2,32749E-14	1,39,685 E-04	3,28354E-07	9,58133E-08	-4,82,332 E-05
$a = 0.7; b = 1.5; c = 0.7$	-4,51305E-13	3,41754E-14	-2,32749E-14	1,39,685 E-04	3,28354E-07	9,58133E-08	-4,82,332 E-05
$a = 0.6; b = 0.9; c = 1.3$	-4,51305E-13	3,41754E-14	-2,32749E-14	1,39,685 E-04	3,28354E-07	9,58133E-08	-4,82,332 E-05
$a = 1.2; b = 0.5; c = 1.3$	-4,51305E-13	3,41754E-14	-2,32749E-14	1,39,685 E-04	3,28354E-07	9,58133E-08	-4,82,332 E-05
$a = 0.5; b = 1.4; c = 0.8$	-4,51305E-13	3,41754E-14	-2,32749E-14	1,39,685 E-04	3,28354E-07	9,58133E-08	-4,82,332 E-05
$a = 1.2; b = 0.6; c = 1.5$	-4,51305E-13	3,41754E-14	-2,32749E-14	1,39,685 E-04	3,28354E-07	9,58133E-08	-4,82,332 E-05
$X = \sigma/\mu(\%)$	0	0	0	0	0	0	0

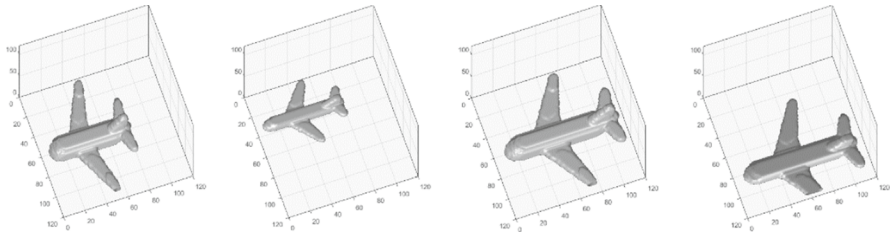


Fig. 9 Set of 3D "Airplane" object transformed by a set of mixed translation and scaling transformations

terms and factorials, unlike the Tchebichef and Krawtchouk polynomials which are defined by the hypergeometric functions ${}_3F_2(\cdot)$ and ${}_2F_1(\cdot)$, respectively.

4.4 3D Object Classification

For validation purposes and as an illustration of the interest of 3DCMITS, this subsection proposes a 3D object classification system to evaluate the performance of the proposed 3DCMITS. The proposed system is based on the proposed 3DCMITS and the Support Vector Machine (SVM) classifier. And to verify the found results, the K-Nearest Neighbor (KNN) classifier is also used in this study.

The performances of classification system based on the proposed 3DCMITS are compared with classification systems based on 3D Legendre moment invariants (3DLMI) [14], 3D Krawtchouk moment invariants (3DKMI) [1], and 3D Tchebichef moment Invariants (3DTMI) [7]. It should be noted that the 3DCMITS based on the indirect method are not considered in this subsection because of their high computation time.

The 3D object classification system consists of four main phases: the data preprocessing phase (training set and test set). Then, the construction phase of the feature vectors. Then, the data classification phase using the SVM classifier, and finally the validation phase and decision-making. The flowchart of the proposed classifier system is presented in Fig. 10 and described as follows:

4.4.1 Phase 1: Data Preprocessing

The McGill 3D Shape Benchmark database [47] is used in this paper to validate the proposed 3DCMITS-based classification system. This database contains 19 different objects and each object has between 20 and 30 exemplars. For each object, the first three samples (Object_1, Object_2, Object_3) of size $128 \times 128 \times 128$ are selected in order to create a base of 57 objects ($19 \text{ classes} \times 3$). Three datasets were constructed for the purpose of this work: (1) Dataset No. 1 includes 1368 objects ($57 \times 24 \text{ instances}$) and is produced by the non-uniform scaling of the 57 objects with the scaling factors $a, b, c \in \{0.5, 0.75, 1.25\}$, the case of $a = b = c$ is not considered. (2) Dataset No. 2 comprises 1539 objects ($190 \times 27 \text{ instances}$) and is produced by translating the 57 objects with the translation vectors $TV(T_x, T_y, T_z)$ where $T_x, T_y, T_z \in \{-6, +2, +10\}$. (3) Dataset No. 3 comprises 3078 objects

Table 3 A comparison of the proposed method and the indirect one in terms of the invariability of 3DCMITS

Method	Translation and scaling	$\Phi_{1,2,0}$	$\Phi_{2,1,0}$	$\Phi_{1,2,1}$	$\Phi_{2,1,1}$	$\Phi_{3,0,0}$	$\Phi_{1,3,1}$	$\Phi_{3,1,1}$	
Proposed	$a = 0.5; b = 0.6; c = 0.7 \Delta i = -8; \Delta j = 6; \Delta k = +8$	-3,07E-13	-1,76E-13	-1,16E-14	0,000,135	2,94E-05	5,26E-05	2,53E-05	
	$a = 0.5; b = 0.8; c = 1.3 \Delta i = 4; \Delta j = +10; \Delta k = -5$	-3,07E-13	-1,76E-13	-1,16E-14	0,000,135	2,94E-05	5,26E-05	2,53E-05	
	$a = 1.7; b = 0.7; c = 1.5 \Delta i = -10; \Delta j = +5; \Delta k = +7$	-3,07E-13	-1,76E-13	-1,16E-14	0,000,135	2,94E-05	5,26E-05	2,53E-05	
	$a = 1; b = 0.8; c = 1.4 \Delta i = +2; \Delta j = +8; \Delta k = +5$	-3,07E-13	-1,76E-13	-1,16E-14	0,000,135	2,94E-05	5,26E-05	2,53E-05	
	$a = 1.3; b = 1.2; c = 0.5 \Delta i = +3; \Delta j = -4; \Delta k = +10$	-3,07E-13	-1,76E-13	-1,16E-14	0,000,135	2,94E-05	5,26E-05	2,53E-05	
	$a = 1.3; b = 0.8; c = 0.7 \Delta i = +10; \Delta j = +7; \Delta k = -4$	-3,07E-13	-1,76E-13	-1,16E-14	0,000,135	2,94E-05	5,26E-05	2,53E-05	
	$X = \sigma/\mu(\%)$	2,19E-10	1,525E-09	0	3,31E-10	4,564E-11	0	1,496E-14	
	Average of X	3,03E-10							
	Indirect	$a = 0.5; b = 0.6; c = 0.7 \Delta i = -8; \Delta j = 6; \Delta k = +8$	-7,19E-13	-5,98E-14	5,30E-14	0,00,012	-2,33E-07	-5,43E-07	9,99E-05
		$a = 0.5; b = 0.8; c = 1.3 \Delta i = 4; \Delta j = +10; \Delta k = -5$	-7,19E-13	-5,98E-14	5,30E-14	0,00,012	-2,33E-07	-5,43E-07	9,99E-05
$a = 1.7; b = 0.7; c = 1.5 \Delta i = -10; \Delta j = +5; \Delta k = +7$		-7,19E-13	-5,98E-14	5,30E-14	0,00,012	-2,33E-07	-5,43E-07	9,99E-05	
$a = 1; b = 0.8; c = 1.4 \Delta i = +2; \Delta j = +8; \Delta k = +5$		-7,19E-13	-5,98E-14	5,30E-14	0,00,012	-2,33E-07	-5,43E-07	9,99E-05	
$a = 1.3; b = 1.2; c = 0.5 \Delta i = +3; \Delta j = -4; \Delta k = +10$		-7,19E-13	-5,98E-14	5,30E-14	0,00,012	-2,33E-07	-5,43E-07	9,99E-05	
$a = 1.3; b = 0.8; c = 0.7 \Delta i = +10; \Delta j = +7; \Delta k = -4$		-7,19E-13	-5,98E-14	5,30E-14	0,00,012	-2,33E-07	-5,43E-07	9,99E-05	
$X = \sigma/\mu(\%)$		5,754E-14	7,477E-09	1,331E-14	0,0,007,484	7,687E-06	2,469E-05	8,934E-12	
Average of X		1,1219E-4							

Table 4 The Average times (s) of the 3DCMIT for the 3D objects using the proposed method and the indirect one

Translation factor	Proposed method			Indirect method		
	Order 12	Order 24	Order 36	Order 12	Order 24	Order 36
- 1	0,05	0,98	1,81	55,77	209,05	751,58
0	0,11	1,1	1,98	56,35	211,55	743,04
1	0,04	1,03	2,04	54,93	208,26	741,79
2	0,04	1,12	2,65	55,86	215,25	742,1
Average time	0,06	1,058	2,12	55,728	211,03	744,63
Total average time	1,08			337,13		
ETIR (%)	99,67%					

Bold indicates the best results obtained in the experimental study

Table 5 The Average times (s) of the 3DCMIS for the 3D objects using the proposed method and the indirect one

Scaling factor	Proposed method			Indirect method		
	Order 12	Order 24	Order 36	Order 12	Order 24	Order 36
0.5	0,0075	0,022	0,074	5,27	68,12	364,35
1	0,013	0,099	0,17	54,78	213,05	743,98
1.5	0,034	0,10	0,19	186,47	393,5	913,5
2	0,09	0,22	0,39	306,47	834,13	1528,5
Average time	0,036	0,11	0,206	138,25	377,2	887,58
Total average time	0,117			467,67		
ETIR (%)	99,97%					

Bold indicates the best results obtained in the experimental study

Table 6 Average times (s) and reduction percentage of invariant moments for transformed 3DMRI

Descriptors	Average time computation (s) of invariant moments using		
	Direct method	Indirect method	ETIR (%)
3DCMITS	0,0135	58,72	99,97%
3DTMI [7]	0,585	67,36	99,13%
3DKMI [1]	0,275	61,50	99,55%

Bold indicates the best results obtained in the experimental study

**Fig. 10** 3D Object recognition process

(57×54 instances) and is generated with mixed translation and scale transformations of the 57 objects using translation vectors $TV(T_x, T_y, T_z)$ where $T_x, T_y, T_z \in \{-6, +6\}$ and scaling factors $a, b, c \in \{0.75, 1.5\}$, respectively. Finally, the salt-and-pepper noise is added in the three datasets mentioned above with the densities $\{1\%, 2\%, 3\%, 4\%\}$. In this paper, we choose 15% of the objects as a training set and the remaining 85% as a test set.

4.4.2 Phase 2: Construction of Feature Vector

The choice of an appropriate characteristic vector is a critical factor to have a high classification rate. For this, we only take into account the first 64 coefficients of the 3DCMITS. The lower order moments choice is justified by their ability to represent the significant characteristics of 3D objects and by their robustness against noise attacks [10]. For each object, the selected coefficients of the 3DCMITS are used to construct the following one-dimensional feature vector:

$$\vec{V} = \{V_1, V_2, V_3, \dots, V_{64}\} \quad (59)$$

Finally, each data object (the training set) is represented by a pair of {Class label, feature vector \vec{V} }.

4.4.3 Phase 3: Classifier

For high correct prediction of test data, the SVM classifier is adopted in this work because of their usefulness for data classification. Based on the training data, the SVM classifier produces a model that predicts the test data labels based on feature vectors of the test data. To avoid the numerical difficulties during computation, the feature vectors are first scaled to put their elements in the range $[-1, +1]$. Another reason for using this normalization is to avoid that feature vectors in larger numerical ranges dominate feature vectors in smaller numerical ranges. As the kernel of the model, the Radial Basis Function (RBF) is chosen in this classification test because of its ability to handle the case where the relationship between class labels and feature vector attributes is nonlinear. In addition, the RBF presents less numerical difficulties and it has only two parameters: penalty parameter C and γ parameter, which does not increase the complexity of the choice of the model unlike other kernels which have a high number of parameters. To identify the best parameters C and γ , cross-validation is first used in our context. Then, the voucher (C, γ) is used to form the training set.

4.4.4 Phase 4: Decision

The accuracy of 3D object recognition is measured by the following Correct Recognition Percentage (CRP):

$$CRP = \frac{\text{Number of correctly classified 3D objects}}{\text{The total of 3D objects used in the test}} \times 100 \quad (60)$$

The classification performance of the proposed 3DCMITS is verified and compared with that of 3DLMI, 3DKMI, and 3DTMI presented in papers [1, 14], and [7], respectively. The classification accuracies based on SVM classifier of sets No. 1, No. 2 and No. 3 are presented in Tables 7, 8 and 9, respectively.

Examining the results of these tables, Table 7 shows that for the case of 3D objects transformed by translation (Dataset No. 1), 3DCMITS, 3DTMI, and 3DKMI lead to high classification rates, with a relative preference for the 3DTMI which present the rate of 87,59%, while the proposed 3DCMITS and 3DKMI present the rates of 87,40% and 87,29%, respectively. In contrast, 3DLMI have the lowest rate with a rate of 79.96%. In Table 8, it is clearly shown that for the case of scaled 3D objects (Dataset No. 2), the proposed 3DCMITS result in the highest classification rates. The 3DCMITS have the highest rate of 86,64%, followed by 3DLMI with 79,12%, while 3DKMI and 3DTMI have the lowest rates of

Table 7 Classification results of the 3D objects with translation transformations using SVM classifier

Descriptors	Noise-free		Salt-and-pepper noise			Average CRP
	0%	1%	2%	3%	4%	
Proposed 3DCMITS	95,72	90,42	87,86	83,55	79,46	87,402
3DLMI [14]	89,46	84,29	79,29	75,14	71,63	79,962
3DKMI [1]	95,63	91,38	87,36	83,07	79,02	87,292
3DTMI [7]	95,52	91,26	87,91	83,72	79,54	87,590

Bold indicates the best results obtained in the experimental study

Table 8 Classification results of the 3D objects with scaling transformations using SVM classifier

Descriptors	Noise-free		Salt-and-pepper noise			Average CRP
	0%	1%	2%	3%	4%	
Proposed 3DCMITS	94,49	90,25	86,71	83,06	78,69	86,640
3DLMI [14]	87,57	83,86	78,77	74,29	71,11	79,120
3DKMI [1]	83,78	79,50	74,97	70,54	67,59	75,276
3DTMI [7]	76,45	73,83	69,60	66,65	63,07	69,920

Bold indicates the best results obtained in the experimental study

Table 9 Classification results of the 3D objects with translation and scaling transformations using SVM classifier

Descriptors	Noise-free		Salt-and-pepper noise			Average CRP
	0%	1%	2%	3%	4%	
Proposed 3DCMITS	91,85	87,72	84,86	80,70	75,81	84,188
3DLMI [14]	83,33	81,17	77,49	73,57	69,82	77,076
3DKMI [1]	81,25	76,76	73,36	69,07	65,50	73,188
3DTMI [7]	74,73	70,52	67,52	63,94	60,52	67,446

Bold indicates the best results obtained in the experimental study

Table 10 Classification results of the 3D objects with translation transformations using KNN classifier

Descriptors	Noise-free		Salt-and-pepper noise			Average CRP
	0%	1%	2%	3%	4%	
Proposed 3DCMITS	91,85	87,71	84,16	80,29	75,06	83,814
3DLMI [14]	85,53	79,64	75,25	71,04	67,82	75,856
3DKMI [1]	91,52	87,35	84,03	80,17	74,95	83,604
3DTMI [7]	91,43	87,65	84,27	80,35	75,24	83,788

Bold indicates the best results obtained in the experimental study

Table 11 Classification results of the 3D objects with scaling transformations using KNN classifier

Descriptors	Noise-free		Salt-and-pepper noise			Average CRP
	0%	1%	2%	3%	4%	
Proposed 3DCMITS	86,47	81,89	76,38	72,70	69,93	77,474
3DLMI [14]	81,53	77,54	73,27	68,02	64,65	73,002
3DKMI [1]	79,62	74,21	70,05	64,85	62,52	70,250
3DTMI [7]	73,48	67,73	65,16	61,28	58,95	65,320

Bold indicates the best results obtained in the experimental study

75,28% and 69,92%, respectively. This is mainly due to the method of extracting the scale invariants of 3D moments of Krawtchouk and Tchebichef, respectively. The advantages of the proposed descriptors are clearly highlighted when dataset No. 3 is used: Table 9 shows that for the case of mixed translation and scaling transformations, 84,19% of 3D objects are classified correctly using the proposed 3DCMITS, while 77,08%, 73,19%, and 67,45% for the 3DLMI, 3DKMI, and 3DTMI, respectively. It should be noted that recognition accuracy decreases with increasing noise. However, the proposed 3DCMITS have recognition rates in excess of 84% even at high noise intensities. These results show that the proposed Charlier invariant moments are robust to translation and scaling transformations, whose recognition rate is higher than those of the 3D invariant moments of Legendre [14], Krawtchouk [1], and Tchebichef [7].

In order to confirm the above discussions and to validate the results found, the classification process is redone using the K-Nearest Neighbor (KNN) classifier. The Euclidean distance [20] is used for the KNN classifier and the value of the K parameter (number of nearest neighbors) is chosen by varying K until the minimum error is reached. The classification results of datasets No. 1, No. 2 and No. 3, based on the KNN classifier, are presented in Tables 10, 11, and 12, respectively. The results of these tables indicate that the proposed 3DCMITS lead to the highest classification rates and are superior to 3DLMI, 3DKMI, and 3DTMI, which result in the lowest classification rates. These results confirm the previous discussions in terms of the studied descriptors' effectiveness for the 3D object classification. It should also be noted that the results found based on the SVM

Table 12 Classification results of the 3D objects with translation and scaling transformations using KNN classifier

Descriptors	Noise-free		Salt-and-pepper noise			Average CRP
	0%	1%	2%	3%	4%	
Proposed 3DCMITS	84,52	79,34	75,80	71,73	67,26	75,730
3DLMI [14]	79,36	75,23	71,99	66,81	63,01	71,280
3DKMI [1]	76,30	71,11	68,33	63,01	59,38	67,626
3DTMI [7]	70,62	66,65	64,77	60,31	56,31	63,732

Bold indicates the best results obtained in the experimental study

classifier are higher than those based on the KNN classifier: with the proposed 3DCMITS, 87,40%, 86,64%, and 84,19% of objects are well classified using SVM classifier for dataset No. 1, dataset No. 2, and dataset No. 3, respectively. While 83,81%, 77,47%, and 75,73% are well classified using KNN classifier. This is due to the superiority of the SVM which offers satisfactory results in the field of 3D object classification/recognition.

5 Conclusion

In this paper, we have proposed a fast method for calculating the translation and scaling invariants of 3D Charlier moment. This method is based on the extraction of these invariants directly via the Charlier polynomials without any numerical approximation. The calculation of these descriptors using this method allows, on the one hand, to considerably reduce the calculation time with an improvement of 99,97%, and on the other hand, to increase the robustness against translation and scale transformations. The interest of the proposed 3DCMITS is shown in the 3D object recognition application. The noise robustness and recognition accuracy of the proposed 3DCMITS are studied. Experimental results show the efficiency and superiority of the proposed 3DCMITS. These descriptors have a desirable capability for 3D image/object description and can be useful in the image analysis field.

Acknowledgements The authors would like to thank the anonymous referees for their helpful comments and suggestions.

Authors' Contributions *Category 1:* Conception and design of study was performed by M. Y, H K. Acquisition of data was performed by Mohamed Yamni, H K, A D, O E ogri, M S, H Q. Analysis and/or interpretation of data was performed by M. Y, H. K, M. S, H. Q, M. M, B. A. *Category 2:* M. Y, H. K., A. D., O. E. ogri drafted the manuscript. M. Y, M. S, H. Q, M. M, B. A. revised the manuscript critically for important intellectual content. *Category 3:* M. Y, H. K, A. D, O E. ogri, M. S, H. Q, M. M, B. A. were responsible for the approval of the version of the manuscript to be published.

Funding No funding has been granted for this work.

Data Availability The datasets generated in our experiments are available from McGill 3D Shape Benchmark images Database, URL link: <http://www.cim.mcgill.ca/~shape/benchMark/airplane.html>. (2017). Accessed 9 March 2020. The datasets used or analyzed during the current study are available from the corresponding author on reasonable request.

Declarations

Conflict of interests The authors declare that we have no competing interests in the submission of this manuscript.

References

1. R. Benouini et al., Efficient 3D object classification by using direct Krawtchouk moment invariants. *Multimed. Tools Appl.* **77**(20), 27517–27542 (2018)
2. T.J. Bin et al., Subpixel edge location based on orthogonal Fourier-Mellin moments. *Image Vis. Comput.* **26**(4), 563–569 (2008)
3. C.-W. Chong et al., Translation and scale invariants of Legendre moments. *Pattern Recognit.* **37**(1), 119–129 (2004)
4. L. Comtet, *Advanced Combinatorics: The Art of Finite and Infinite Expansions* (Springer Science & Business Media, 2012)
5. O. El ogri et al., 2D and 3D medical image analysis by discrete orthogonal moments. *Procedia Comput. Sci.* **148**, 428–437 (2019)
6. A. Daoui et al., Stable computation of higher order Charlier moments for signal and image reconstruction. *Inf. Sci.* **521**, 251–276 (2020). <https://doi.org/10.1016/j.ins.2020.02.019>
7. M. El Mallahi et al., Translation and scale invariants of three-dimensional Tchebichef moments. in *2015 Intelligent Systems and Computer Vision (ISCV)* (IEEE, 2015), p. 1–5
8. O. El. Ogri et al., New set of fractional-order generalized Laguerre moment invariants for pattern recognition. *Multimed. Tools Appl.* **79**, 23261–23294 (2020)
9. S. Farokhi et al., Near infrared face recognition by combining Zernike moments and undecimated discrete wavelet transform. *Digit. Signal Process.* **31**, 13–27 (2014)
10. J. Flusser et al., *2D and 3D Image Analysis by Moments* (Wiley, Hoboken, 2016)
11. J. Flusser, T. Suk, Pattern recognition by affine moment invariants. *Pattern Recognit.* **26**(1), 167–174 (1993)
12. X. Guo, Three dimensional moment invariants under rigid transformation. in *International Conference on Computer Analysis of Images and Patterns* (Springer, Berlin, Heidelberg, 1993), pp. 518–522
13. K.M. Hosny, Exact and fast computation of geometric moments for gray level images. *Appl. Math. Comput.* **189**(2), 1214–1222 (2007)
14. K.M. Hosny, Fast and low-complexity method for exact computation of 3D Legendre moments. *Pattern Recognit. Lett.* **32**(9), 1305–1314 (2011)
15. K.M. Hosny, Fast computation of accurate Gaussian-Hermite moments for image processing applications. *Digit. Signal Process.* **22**(3), 476–485 (2012)
16. H. Karmouni et al., Fast and stable computation of the Charlier moments and their inverses using digital filters and image block representation. *Circuits Syst. Signal Process.* **37**(9), 4015–4033 (2018)
17. M.K. Hu, Visual pattern recognition by moment invariants. *IRE Trans. Inf. Theory.* **8**(2), 179–187 (1962). <https://doi.org/10.1109/TIT.1962.1057692>
18. R. Mukundan et al., Discrete vs. continuous orthogonal moments for image analysis (2001)
19. R. Mukundan et al., Image analysis by Tchebichef moments. *IEEE Trans. Image Process.* **10**(9), 1357–1364 (2001)
20. R. Mukundan and K.R. Ramakrishnan, *Moment functions in image analysis: theory and applications*. (World Scientific, 1998)
21. A.F. Nikiforov et al., Classical orthogonal polynomials of a discrete variable, in *Classical orthogonal polynomials of a discrete variable*. (Springer, New York, 1991), pp. 18–54

22. P.A. Oliveira et al., A discrete Tehebichef transform approximation for image and video coding. *IEEE Signal Process. Lett.* **22**(8), 1137–1141 (2015)
23. F.A. Sadjadi, E.L. Hall, Three-dimensional moment invariants. *IEEE Trans. Pattern Anal. Mach. Intell.* **PAMI-2**, 127–136 (1980). <https://doi.org/10.1109/TPAMI.1980.4766990>
24. M. Sayyouri et al., A fast and accurate computation of 2D and 3D generalized Laguerre moments for images analysis. *Multimed. Tools Appl.* **80**(5), 7887–7910 (2021)
25. M. Sayyouri et al., A fast computation of novel set of Meixner invariant moments for image analysis. *Circuits Syst. Signal Process.* **34**(3), 875–900 (2015)
26. T. Suk, J. Flusser, Tensor method for constructing 3D moment invariants. in *International Conference on Computer Analysis of Images and Patterns* (Springer, 2011). pp. 212–219
27. C. Wang et al., Image description with polar harmonic Fourier moments. *IEEE Trans. Circuits Syst. Video Technol.* **30**(12), 4440–4452 (2019)
28. C. Wang et al., Quaternion polar harmonic Fourier moments for color images. *Inf. Sci.* **450**, 141–156 (2018)
29. C. Wang et al., Ternary radial harmonic Fourier moments based robust stereo image zero-watermarking algorithm. *Inf. Sci.* **470**, 109–120 (2019)
30. Z. Xia et al., Color medical image lossless watermarking using chaotic system and accurate quaternion polar harmonic transforms. *Signal Process.* **157**, 108–118 (2019)
31. Z. Xia et al., Geometrically invariant color medical image null-watermarking based on precise quaternion polar harmonic fourier moments. *IEEE Access.* **7**, 122544–122560 (2019)
32. B. Xiao et al., Radial shifted Legendre moments for image analysis and invariant image recognition. *Image Vis. Comput.* **32**(12), 994–1006 (2014)
33. D. Xu, H. Li, 3-D affine moment invariants generated by geometric primitives. in *18th International Conference on Pattern Recognition (ICPR'06)* (IEEE, 2006). pp. 544–547
34. D. Xu, H. Li, Geometric moment invariants. *Pattern Recognit.* **41**(1), 240–249 (2008). <https://doi.org/10.1016/j.patcog.2007.05.001>
35. S. Xu et al., Accurate Computation of Fractional-Order Exponential Moments. *Secur. Commun. Netw.* **2020**, 1–6 (2020)
36. M. Yamni et al., Blind image zero-watermarking algorithm based on radial krawtchouk moments and chaotic system. in *2020 International Conference on Intelligent Systems and Computer Vision (ISCV)* (IEEE, 2020). pp. 1–7
37. M. Yamni et al., Color Stereo image zero-watermarking using quaternion radial tchebichef moments. in *2020 International Conference on Intelligent Systems and Computer Vision (ISCV)* (IEEE, 2020). pp. 1–7
38. M. Yamni et al., Fractional Charlier moments for image reconstruction and image watermarking. *Signal Process.* **171**, 107509 (2020)
39. M. Yamni et al., Image watermarking using separable fractional moments of Charlier–Meixner. *J. Frankl. Inst.* **358**(4), 2535–2560 (2021). <https://doi.org/10.1016/j.jfranklin.2021.01.011>
40. M. Yamni et al., Novel Octonion Moments for color stereo image analysis. *Digit. Signal Process.* **108**, 102878 (2021). <https://doi.org/10.1016/j.dsp.2020.102878>
41. P.-T. Yap et al., Image analysis by Krawtchouk moments. *IEEE Trans. Image Process.* **12**(11), 1367–1377 (2003)
42. R. Zhi et al., Translation and scale invariants of Krawtchouk moments. *Inf. Process. Lett.* **130**, 30–35 (2018)
43. J. Zhou Jian et al., Image analysis by discrete orthogonal Hahn moments. in *International Conference Image Analysis and Recognition* (Springer, Berlin, Heidelberg, 2005). p. 524–531
44. H. Zhu et al., Image analysis by discrete orthogonal Racah moments. *Signal Process.* **87**(4), 687–708 (2007)
45. H. Zhu et al., Image description with nonseparable two-dimensional charlier and meixner moments. *Int. J. Pattern Recognit. Artif. Intell.* **25**(01), 37–55 (2011). <https://doi.org/10.1142/S0218001411008506>
46. H. Zhsu et al., Translation and scale invariants of Tehebichef moments. *Pattern Recognit.* **40**(9), 2530–2542 (2007)
47. McGill 3D Shape Benchmark, <http://www.cim.mcgill.ca/~shape/benchMark/>, last accessed 2020/03/09

Publisher's Note Springer Nature remains neutral with regard to jurisdictional claims in published maps and institutional affiliations.

Authors and Affiliations

M. Yamni¹  · **A. Daoui**² · **O. El ogri**¹ · **H. Karmouni**¹ · **M. Sayyouri**² · **H. Qjidaa**¹ · **M. Maaroufi**^{3,4} · **B. Alami**^{3,4,5}

A. Daoui
achraf.daoui@usmba.ac.ma

O. El ogri
omar.elogri@usmba.ac.ma

H. Karmouni
hicham.karmouni@usmba.ac.ma

M. Sayyouri
mhamed.sayyouri@usmba.ac.ma

H. Qjidaa
qjidah@yahoo.fr

M. Maaroufi
mustapha.maaroufi@usmba.ac.ma

B. Alami
badreeddine.alami@usmba.ac.ma

¹ Faculty of Science Dhar El Mahrez, Laboratory of Electronic Signals and Systems of Information LESSI, CED-ST, STIC, University Sidi Mohamed Ben Abdellah, Fez, Morocco

² Engineering, Systems and Applications Laboratory, National School of Applied Sciences, Sidi Mohamed Ben Abdellah University, BP 72, My Abdallah Avenue Km. 5 Imouzzar Road, Fez, Morocco

³ Faculty of Medicine and Pharmacy, Clinical Neuroscience Laboratory, Sidi Mohamed Ben Abdellah University, Fez, Morocco

⁴ Department of Radiology and Clinical Imaging, University Hospital of Fez, Fez, Morocco

⁵ Department of Biophysics and Clinical MRI Methods, Sidi Mohamed Ben Abdellah University, Km 2.200, Sidi Hrazem Road, BP. 893, 30000 Fez, Morocco